RSC Advances

PAPER

View Article Online
View Journal | View Issue

Cite this: *RSC Adv.*, 2023, **13**, 3534

Novel albumin-binding photodynamic agent EB-Ppa for targeted fluorescent imaging guided tumour photodynamic therapy†

Huan Liu, ‡[a] Cheng Yu,‡[a] Min Lyu,[a] Shiyi Lyu,[a] LiNan Hu,*[b] Enhua Xiao*[a] and Pengfei Xu *[cd]

Received 20th November 2022
Accepted 13th January 2023

DOI: 10.1039/d2ra07380c

rsc.li/rsc-advances

The targeted and novel albumin-binding strategy has been attractive in the field of cancer therapy. Herein, we have developed an organic small molecule-based photosensitizer, Evans Blue-Pyropheophorbide-alpha (EB-Ppa), to treat solid tumors with extremely high photodynamic therapeutic efficiency, which is stable in serum-containing aqueous media and can effectively accumulate in the tumor site due to the enhanced permeability and retention (EPR) effect. Particularly, after the photodynamic therapeutic treatment with EB-Ppa, all breast tumors (4T1 cell line) xenografted in nude mice shrink fast due to the singlet oxygen generated by EB-Ppa with laser irradiation. Furthermore, EB-Ppa shows negligible toxicity in major organs. These results demonstrate that EB-Ppa presents the great potential of photodynamic therapy for efficient tumor treatment.

Introduction

Cancer is ranked as the leading cause of death and an important public health problem worldwide with a heavy disease burden.[1,2] To deal with such a challenge, some traditional therapies such as surgery, chemotherapy, and radiotherapy, have been applied in clinics.[3–5] However, given the limited efficacy, drug resistance, and side effects of such traditional cancer treatments, the development of safer and more efficient cancer treatments has been a common goal of multiple disciplines.[6] Photodynamic therapy (PDT), a novel treatment of cancer therapy, has gained tremendous attention in the past decade because of the negligible side effects, and low toxicity compared to the limitations of the above therapeutic methods.[5,7] PDT uses photosensitizers to absorb photons and excite electrons into the excited singlet state under light exposure, then the singlet photosensitizer releases the energy back to the ground state by emitting fluorescence, or converts it into a stable triplet state by intersystem crossing.[8,9] The latter can produce various ROS, including superoxide anion radicals, hydrogen peroxide, and hydroxyl radicals (Type I process), or transfer the energy to molecular oxygen to produce singlet oxygen (Type II process), which can damage the surrounding organelles and biomolecules, causing cell necrosis, apoptosis, autophagy, vascular injury, and immune activation.[10,11]

In order to efficiently destroy the cancer cells, ideal PSs with high absorption coefficients and high singlet oxygen quantum yield are needed. Nevertheless, a great number of conventional PSs are hydrophobic and tend to aggregate in a physiological environment, which often inclines to fluorescence quenching and insufficient ROS production due to the aggregation-caused quenching (ACQ) phenomenon, thus hindering the clinical application of PSs.[12,13] In recent years, pyropheophorbide-a (Ppa) is emerging as a promising PS with a large extinction coefficient ($\varepsilon = 3.79 \times 10^4$ L (mol^{-1} cm^{-1})) and high singlet oxygen quantum yield (>50%).[14] However, concentration quenching of the excited state is a common problem that affects the ROS generation efficiency of Ppa. When used in a physiological environment, Ppa tends to aggregate in aqueous media due to its' rigid planar structure and limited water solubility, which results in impaired singlet oxygen production and severe fluorescence quenching, leading to significantly decreased fluorescence and photodynamic efficiency. Furthermore, Ppa has a very limited tumor-accumulation ability and water solubility, thus restricting its clinical applications.[15–17]

To enhance the availability of Ppa in a physiological environment, various nanocarriers have been employed to encapsulate Ppa to achieve better water dispersibility.[18–20] Unfortunately, the singlet oxygen generation efficiency of Ppa in nanocarriers is often suppressed due to excited state quenching. Moreover, the clinical translation of nano photosensitizers

[a]*Departments of Radiology, The Second Xiangya Hospital, Central South University, Changsha 410011, Hunan, P. R. China. E-mail: xiaoenhua64@csu.edu.cn*

[b]*Departments of Radiology, Zhuzhou Central Hospital, Zhuzhou 412000, Hunan, P. R. China*

[c]*Institute of Clinical Pharmacy & Pharmacology, Jining First People's Hospital, Jining Medical University, Jining 272000, P. R. China*

[d]*Department of Diagnostic Radiology Yong Loo Lin School of Medicine, National University of Singapore, 119074, Singapore*

† Electronic supplementary information (ESI) available. See DOI: https://doi.org/10.1039/d2ra07380c

‡ These authors contributed equally to this work.

has been hampered by complications in large-scale manufacturing, quality control and safety.[21,22]

Because of its natural properties as a blood transporter, human serum albumin (HSA) has been used as a natural carrier for hydrophobic drugs and photosensitizers.[23,24] Albumin is synthesized by the liver and is the most abundant plasma protein (35–50 g L^{-1} human serum) with an average half-life of 19 days.[25,26] Albumin's chemical structure and conformation allow the incorporation of photosensitizers by covalent binding or noncovalent interaction. These properties as well as its preferential uptake in tumor and inflamed tissue, its ready availability, its biodegradability, and its lack of toxicity and immunogenicity make it an ideal candidate for photosensitizer delivery.[27–30]

The ability of albumin-based delivery to improve tumor targeting and accumulation is what makes it effective.[31,32] Increased absorption is the cause of the increased tumor accumulation, which is passively mediated *via* enhanced permeation and retention (EPR).[33] Additionally, albumin can also strengthen the binding and internalization of nanoparticles by attaching to certain receptors that are overexpressed on cancer cells. For instance, the 60 kDa glycoprotein (gp60) receptor and secreted protein acidic and rich in cysteine (SPARC) are overexpressed in a variety of tumors.[34,35] However, the EPR effect remains the main way to improve tumor targeting and accumulation, which inclines to accumulate in tumors significantly more than in normal tissue due to the leaky tumor vasculature and lymphatic outflow.[36,37] This specific uptake mechanism makes albumin-based nanoparticles avoid the drug efflux pathways.

It could be wise to conjugate Ppa with HSA in order to enhance Ppa's physical characteristics. Besides, it can also facilitate the internalization of Ppa into the tumor, boosting Ppa's tumor accumulation and selectivity.[17,18,20] A higher buildup of photosensitizers can boost their reactivity to relatively low-intensity excitation light in deeper places, which is advantageous for the treatment of larger, more deeply embedded tumors, and the damage to nearby normal tissues will also be lessened.[38] Such an approach could address the Ppa-related issues of tumor enrichment and water solubility.

In this work, we developed a novel photosensitizer (EB-Ppa), which binds with albumin in a non-covalent manner *via* hydrogen bond and hydrophobic interactions. EB has a high affinity with serum albumin as an azo dye and non-toxic biological vessel stain.[39,40] The introduction of hydrophilic truncated Evans Blue affords EB-Ppa with good water solubility. After IV injection, EB-Ppa can spontaneously bind with albumin. Thus, the complex can take advantage of EPR effect and endogenous albumin transport pathways for tumor accumulation. *In vivo* fluorescence imaging experiment results reveals higher tumor uptake of EB-Ppa than free Ppa after intravenous administration. In addition, EB-Ppa exhibits good biocompatibility and excellent singlet oxygen generation capability upon 660 nm laser irradiation. *In vitro* and *in vivo* experiments indicates that EB-Ppa achieves significant tumor destruction through the cytotoxic effect of singlet oxygen. In conclusion, we exhibit a highly efficient multifunctional albumin-binding photodynamic agent EB-Ppa with great potential for image-guided PDT.

Results and discussion

Preparation and characterization of EB-Ppa

The synthetic route for EB-Ppa was shown in Scheme 1. EB-Ppa was readily synthesized through the direct conjugation of the carboxylic acid group of NIC with amino group of Compound 1. The structure of EB-Ppa was characterized by UV/vis and MS (Fig. S1†).

Measurement of singlet oxygen

RNO-ID experiment was used to verify singlet oxygen generated by EB-Ppa upon laser irradiation, different solutions, including Ppa, EB-Ppa, and RNO, were irradiated for 10 minutes by a 660 nm laser at a power density of 1.0 W cm^{-2}. As shown in Fig. 1A, upon continuous irradiation with 660 nm laser at 1.0 W cm^{-2} for 10 minutes, the EB-Ppa was capable of rapidly generating singlet oxygen with the increase of concentration, inducing a significant decline in the absorption of RNO, while the Ppa showed the lower ability to generate singlet oxygen compared to the EB-Ppa group. Specifically, the singlet of 200 mg mL^{-1} suspension of EB-Ppa remarkably declined, which was high enough to kill tumor cells *via* photodynamic effect. Similarly, Fig. 1B also showed that EB-Ppa was the highest production of singlet oxygen after 10 minutes of irradiation. Therefore, it was considered that the irradiated EB-Ppa could actively generate singlet oxygen that reacts with RNO.

Cell viability and *in vitro* anti-tumor efficacy

The next series of cell viability experiments were performed to evaluate the *in vitro* cytotoxic effect of EB-Ppa through the CCK-8 assay in 4T1 cells. As is shown in Fig. 2A, after incubation with EB-Ppa plus HSA for 24 h, no obvious toxicity was observed on 4T1 cells even at the highest concentration of 200 mg mL^{-1} (cell viability was above 90%). The results illustrate that EB-Ppa possesses extremely low biotoxicity *in vitro*.

Next, to assess the *in vitro* phototoxicity effects of the EB-Ppa plus laser as compared to free EB-Ppa. 4T1 cells were incubated with different concentrations of EB-Ppa for 24 h, with or without laser irradiation and their viabilities were evaluated by CCK-8 assay. Just as Fig. 2B anticipated, the phototoxicity effect of the EB-Ppa plus laser group was concentration-dependent with decreasing cell viability at increasing concentrations. The cytotoxicity of EB-Ppa was obviously enhanced upon laser irradiation, because EB-Ppa could be activated by laser irradiation to generate singlet oxygen, causing effective apoptosis of tumor cells. Specifically, the cell viability was less than 10% under 200 μg mL^{-1} at 0.5 W cm^{-2} for 5 minutes.

Tumor-targeted fluorescence imaging and biodistribution *in vivo*

To investigate the biodistribution and tumor-targeting ability of EB-Ppa *in vivo*, the free Ppa and EB-Ppa were intravenously injected into 4T1 tumor-bearing mice when the length of the

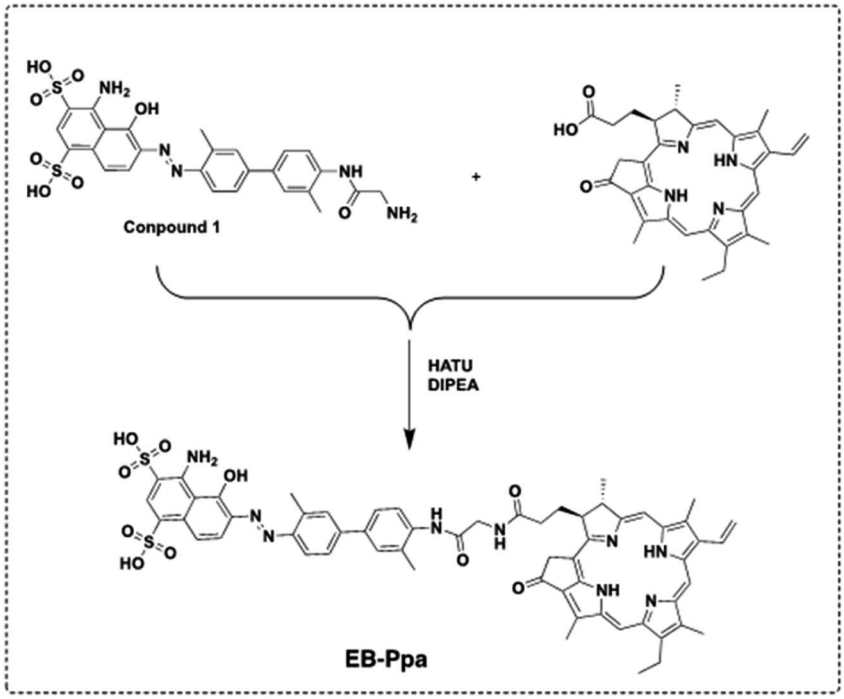

Scheme 1 The structure and synthesize route of probe EB-Ppa.

tumor reached 200–300 mm^3. And then time-dependent accumulations of both Ppa and EB-Ppa were monitored by a bio-imaging system.

As displayed in Fig. 3A, it was observed that the EB-Ppa started to accumulate in the tumor region at 4 h post-injection, and finally reached the maximum at 24 h. Besides, the fluorescence images of Ppa showed a relatively weaker signal in the tumor area compared to the EB-Ppa, due to the fast blood clearance and the relatively poor tumor accumulation, which demonstrated a higher accumulation of EB-Ppa in the tumor re-gion than Ppa. Moreover, the enhanced accumulation of EB-Ppa might be attributed to the stable interaction of EB-Ppa with serum albumin, thus prolonging circulation stability and promoting preferential accumulation inside the tumor *via* EPR effect. Meanwhile, EB-Ppa was mostly distributed in the liver, indicating that the liver was the main organ for drug metabolism and elimination.

An *ex vivo* analysis of the excised tumor and organs were performed after 48 h post-injection and visualized (Fig. 3B). As expected, the tumor displayed the highest fluorescence intensity in the EB-Ppa group, while in the Ppa group, few fluorescence was detected in the tumor (Fig. 3C). All these results demonstrated that EB-Ppa was highly capable of accumulating in the tumor *via* the EPR effect. Furthermore, the weak fluorescence intensity of the major organs, such as the heart, liver, spleen, lung and kidney, furtherly validated the tumor-oriented accumulation of EB-Ppa. The above results indicated that EB-Ppa could effectively reveal its distribution, and target the tumor to realize efficient PDT.

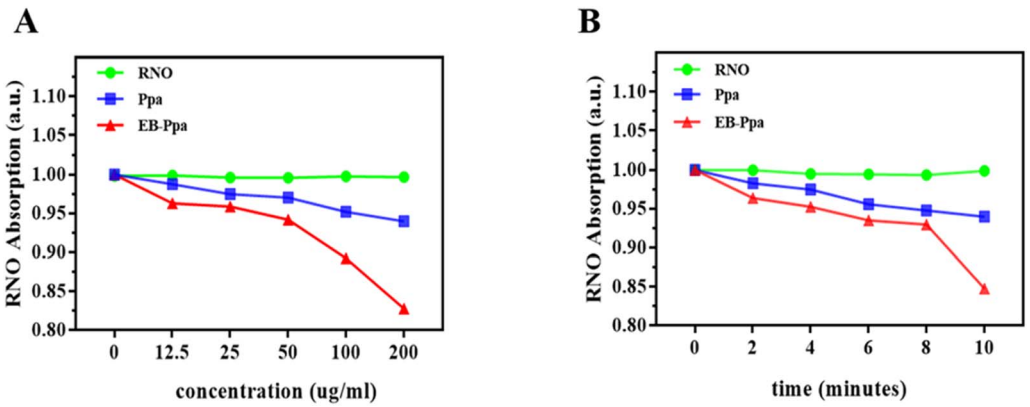

Fig. 1 The singlet oxygen production in EB-Ppa under different concentrations (A) and times (B).

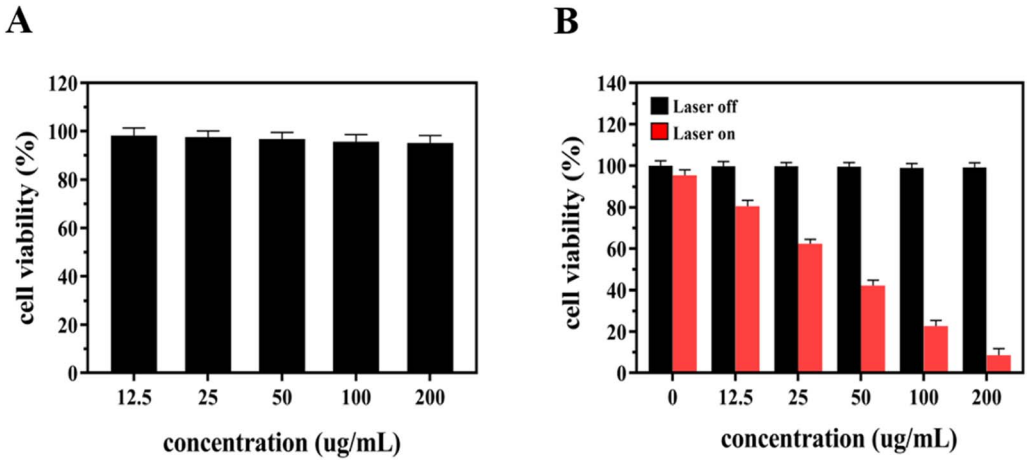

Fig. 2 (A) Cell viability of 4T1 cells after incubation with EB-Ppa at different concentrations for 24 h. (B) The viability of 4T1 cells after incubation with EB-Ppa with or without laser irradiation at different concentrations for 24 h.

In vivo photodynamic therapy

In this study, the *in vivo* anti-tumor efficiency of EB-Ppa was evaluated using a subcutaneous xenograft 4T1 tumor model in nude mice. Based on the biodistribution results *in vivo*, laser irradiation treatments were applied at 24 h post-injection when the accumulation of EB-Ppa at the tumor site reached the maximum. Fig. S2A† showed the tumor growth profiles of 4 different treated groups over a 14 days period. Tumors treated with PBS only, laser only, and EB-Ppa kept a natural growth

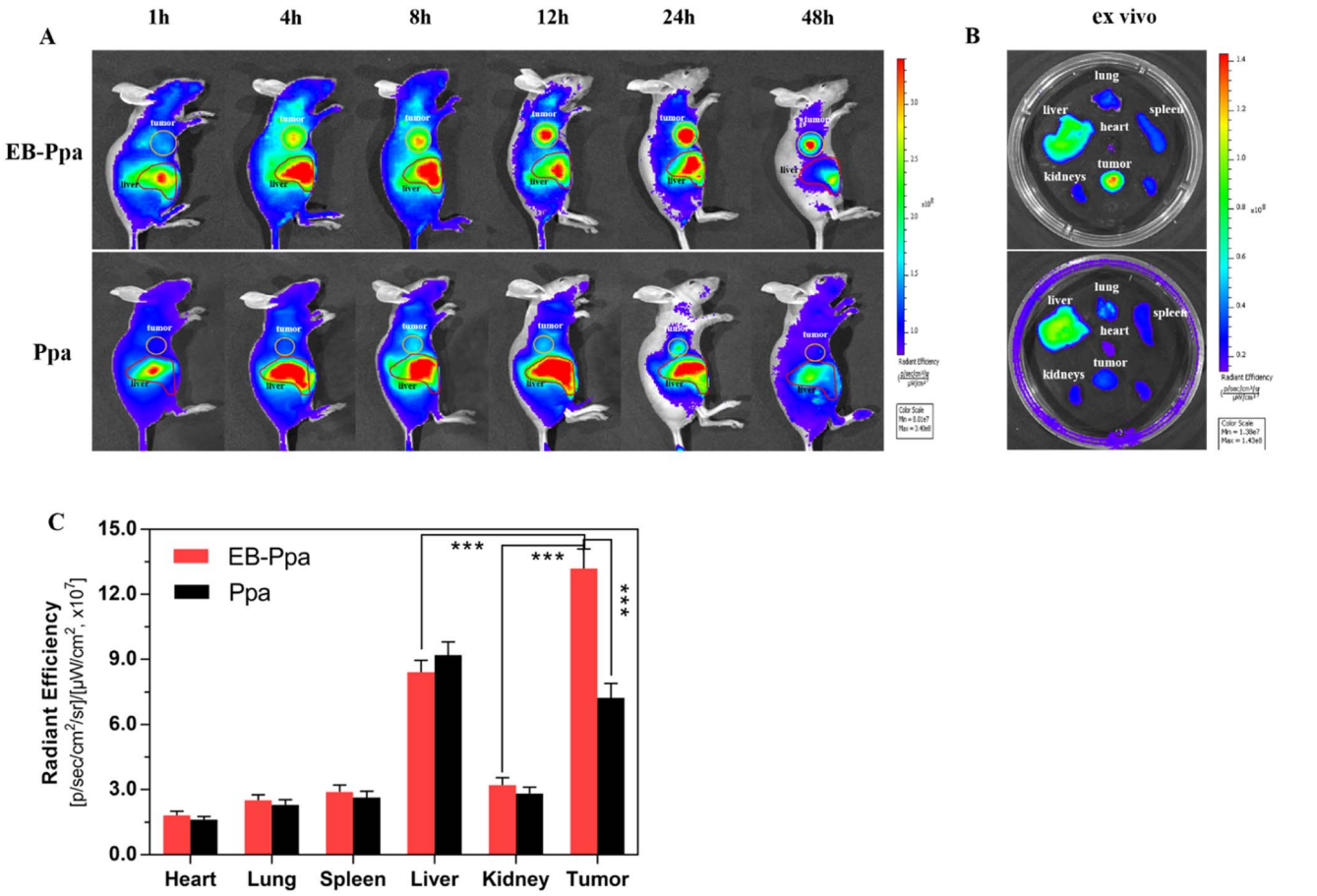

Fig. 3 (A) *In vivo* fluorescence imaging and biodistribution analysis of mice bearing 4T1 tumors treated with Ppa and EB-Ppa. (B) *Ex vivo* fluorescence images of tumors and major organs after 48 h injection (the tumor and liver are circled with a yellow, red circle line, respectively). (C) Quantification of the fluorescent signals on corresponding organs and tumors. Data are given as mean ± SD ($n = 3$). $^{**}p < 0.01$ and $^{***}p < 0.001$.

trend, while EB-Ppa plus laser exhibited excellent photodynamic therapy effect. As is shown in Fig. S2B,† no body weight loss was observed for all four groups during the treatment period, implying no adverse effects from the PDT treatment. Moreover, Fig. 4A and B showed representative photographs of tumor size in different groups, which were consistent with the tumor growth data in Fig. S2A.†

To further validate the anti-tumor efficacy of EB-Ppa, the H&E staining, TUNEL, and PCNA of the tumor tissue sections in different groups were analyzed 14 days post-treatment. It was clearly observed that H&E staining tumor sections of the PBS, laser, and EB-Ppa only groups were evenly distributed, and the nuclei were no observable cell damage (Fig. 4C, top panel), while apparent nucleus dissociation and necrosis, fragmented cell membrane were observed in EB-Ppa plus laser group. Additionally, the TUNEL results indicated that the apoptotic cells of tumor tissues had significantly increased in EB-Ppa plus laser group, but not in other groups, which was consistent with the H&E staining results (Fig. 4C, middle panel). Furthermore, PCNA results showed that the proliferation capacity of tumor tissue was obviously reduced in EB-Ppa plus laser group compared to the other groups (Fig. 4C, bottom panel). All these above results confirmed that EB-Ppa plus laser irradiation method has good performance in tumor PDT.

Biosafety

Biosafety is an extremely important experiment in the clinical application of drugs. Therefore, we assessed the potential toxicity of EB-Ppa *in vivo* ($n = 3$ per group). The biosafety of EB-Ppa was evaluated by H&E staining of the major organs (heart, liver, spleen, lungs, and kidneys) and serum biochemical analysis after treatment. As shown in Fig. 5, normal histological structures were observed in the PBS-treated group, and we did not notice any obvious signs of organ damage in other groups. Moreover, to investigate the hepatotoxicity (levels of ALT, AST), and nephrotoxicity (the levels of BUN, CRE) of the EB-Ppa,

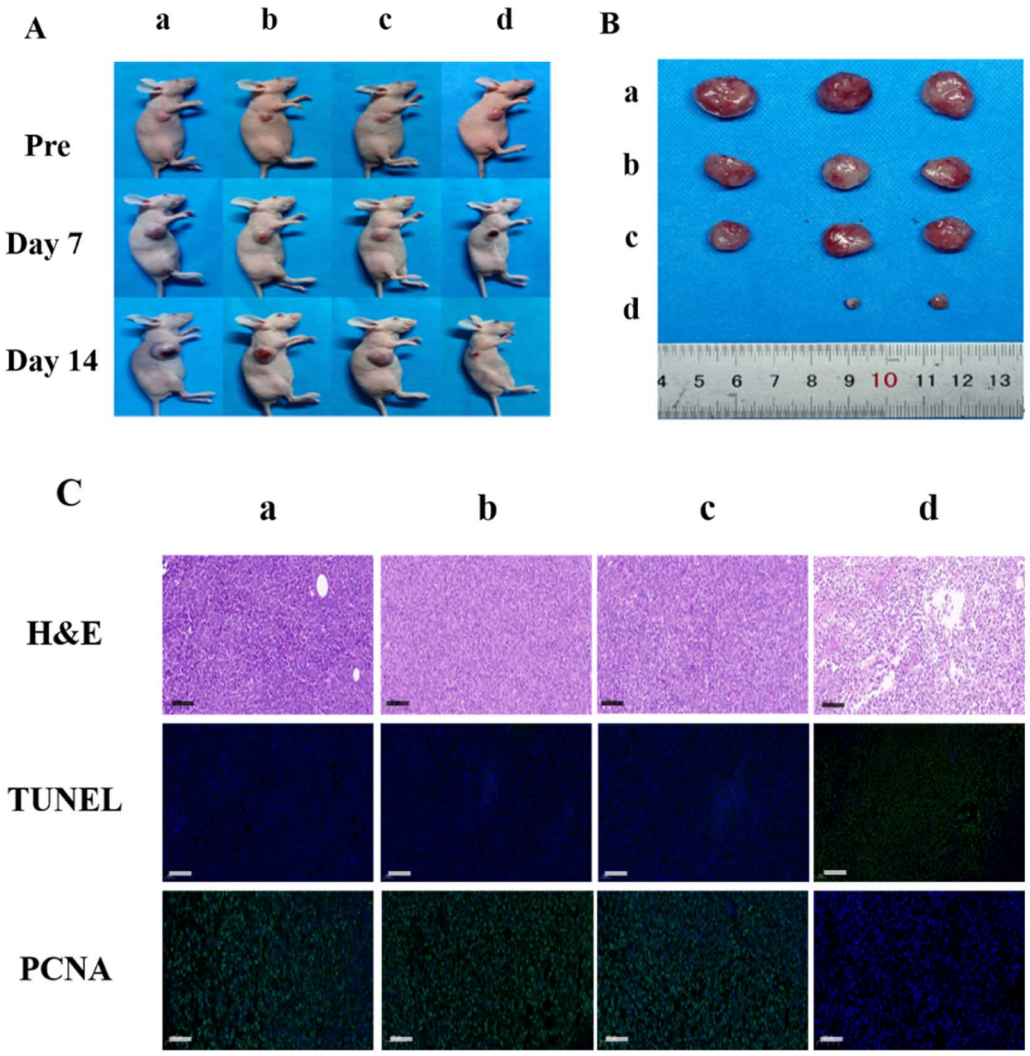

Fig. 4 (A) Variations in photographs of the mice treated with PBS, laser, EB-Ppa with or without laser irradiation (660 nm, 1.0 W cm^{-2}, 10 minutes). (B) The morphology of the treated tumors excised in different groups on day 14. (C) H&E staining, TUNEL and PCNA immunohistochemical staining of the excised tumor tissues. (a) PBS, (b) laser, (c) EB-Ppa, and (d) EB-Ppa + laser, respectively. Scale bar = 100 μm.

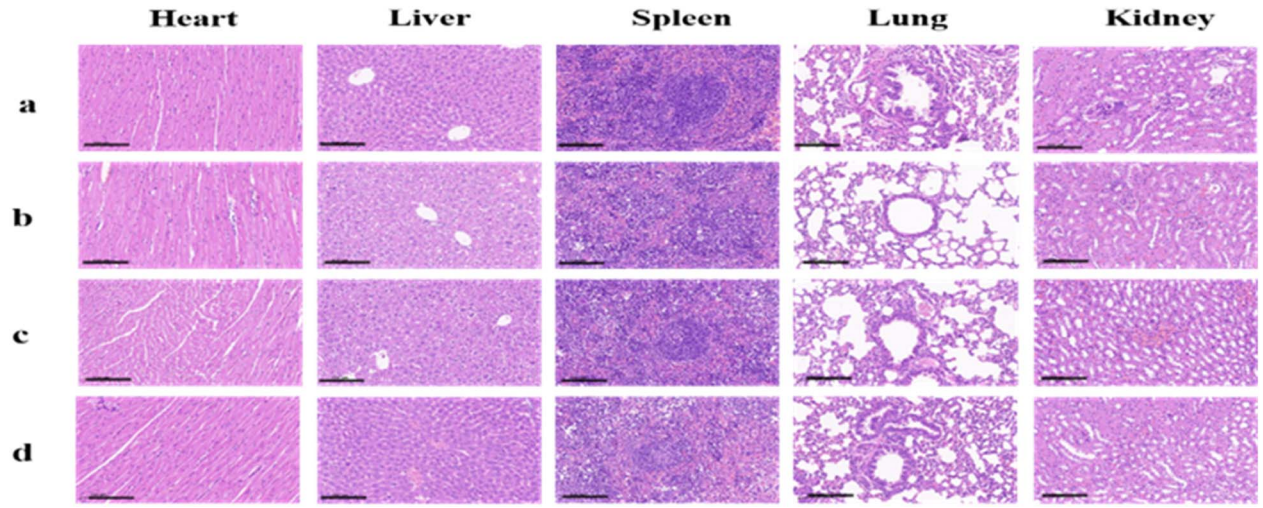

Fig. 5 The H&E staining of the mice treated with PBS as control (a), laser only (b), EB-Ppa and EB-Ppa with laser irradiation treatment (c and d). Scale bar = 100 μm.

serum biochemical analyses were performed (Fig. S3†). Compared with the PBS-treated group, other groups showed no significant adverse effects or acute injury in liver and kidney function index for each group. The above results furtherly indicated that it was potentially safe for EB-Ppa in PDT.

Conclusion

In this work, a novel, superior albumin-binding photodynamic agent EB-Ppa is successfully developed and constructed for targeting tumor imaging and treating the solid tumor with extraordinarily high efficiency. *In vivo* experiments demonstrate that EB-Ppa could efficiently accumulate inside tumors as a result of the EPR effect and obviously suppress the growth of the solid tumors. Additionally, the biosafety experiment reveals negligible toxicity of EB-Ppa toward main organs. Collectively, our studies show that EB-Ppa is an excellent albumin-binding photodynamic agent with a promising clinical application prospect for the treatment of solid tumors, and furtherly confirm that laser-induced PDT is a promising modality to fight against cancer.

Ethical statement

All animal procedures were performed in accordance with the Guidelines for Care and Use of Laboratory Animals of Central South University and approved by the Animal Ethics Committee, The Second Xiangya Hospital, Central South University, China.

Author contributions

Enhua Xiao, Pengfei Xu, LiNan Hu: conceptualization, project administration, supervision, validation, funding acquisition. Huan Liu: methodology, formal analysis, data curation, investigation, writing – original draft preparation. Cheng Yu: methodology, formal analysis, writing – review & editing. Min Lyu Shiyi Lyu: formal analysis.

Conflicts of interest

There are no conflicts of interest to declare. All authors have given approval to the final version of the manuscript.

Acknowledgements

This work was supported by Clinical Research Center for Medical Imaging in Hunan Province (grant no. 2020SK4001), the National Natural Science Foundation of China (grant no. 81571784), Joint Project between Provincial Natural Science Foundation and Science and technology of Hunan (grant no. 2022JJ70142), the Natural Science Foundation of Hunan Province (grant no. 2019JJ40444), China. Shandong Provincial Natural Science Foundation (grant no. ZR2022MH099).

Notes and references

1 F. Bray, M. Laversanne, E. Weiderpass and I. Soerjomataram, *Cancer*, 2021, **127**, 3029–3030.
2 H. Sung, J. Ferlay, R. L. Siegel, M. Laversanne, I. Soerjomataram, A. Jemal and F. Bray, *Ca-Cancer J. Clin.*, 2021, **71**, 209–249.
3 G. N. Hortobagyi and A. U. Buzdar, *Ca-Cancer J. Clin.*, 1995, **45**, 199–226.
4 V. Schirrmacher, *Int. J. Oncol.*, 2019, **54**, 407–419.
5 L. Cheng, C. Wang, L. Feng, K. Yang and Z. Liu, *Chem. Rev.*, 2014, **114**, 10869–10939.
6 J. A. Kemp and Y. J. Kwon, *Nano Convergence*, 2021, **8**, 34.
7 U. Chitgupi, Y. Qin and J. F. Lovell, *Nanotheranostics*, 2017, **1**, 38–58.
8 J. Chen, T. Fan, Z. Xie, Q. Zeng, P. Xue, T. Zheng, Y. Chen, X. Luo and H. Zhang, *Biomaterials*, 2020, **237**, 119827.

9 Z. Xie, T. Fan, J. An, W. Choi, Y. Duo, Y. Ge, B. Zhang, G. Nie, N. Xie, T. Zheng, Y. Chen, H. Zhang and J. S. Kim, *Chem. Soc. Rev.*, 2020, **49**, 8065–8087.
10 J. Xie, Y. Wang, W. Choi, P. Jangili, Y. Ge, Y. Xu, J. Kang, L. Liu, B. Zhang, Z. Xie, J. He, N. Xie, G. Nie, H. Zhang and J. S. Kim, *Chem. Soc. Rev.*, 2021, **50**, 9152–9201.
11 T. Hu, Z. Wang, W. Shen, R. Liang, D. Yan and M. Wei, *Theranostics*, 2021, **11**, 3278–3300.
12 L. E. Bennett, K. P. Ghiggino and R. W. Henderson, *J. Photochem. Photobiol., B*, 1989, **3**, 81–89.
13 M. Kang, C. Zhou, S. Wu, B. Yu, Z. Zhang, N. Song, M. M. S. Lee, W. Xu, F. J. Xu, D. Wang, L. Wang and B. Z. Tang, *J. Am. Chem. Soc.*, 2019, **141**, 16781–16789.
14 Y. H. Gao, X. X. Zhu, W. Zhu, D. Wu, D. Y. Chen, Y. J. Yan, X. F. Wu, D. F. O'Shea and Z. L. Chen, *Eur. J. Med. Chem.*, 2020, **187**, 111959.
15 N. Sekkat, H. van den Bergh, T. Nyokong and N. Lange, *Molecules*, 2011, **17**, 98–144.
16 M. Zhang, Z. Zhang, D. Blessington, H. Li, T. M. Busch, V. Madrak, J. Miles, B. Chance, J. D. Glickson and G. Zheng, *Bioconjugate Chem.*, 2003, **14**, 709–714.
17 A. M. Bugaj, *Photochem. Photobiol. Sci.*, 2011, **10**, 1097–1109.
18 M. Mitsunaga, M. Ogawa, N. Kosaka, L. T. Rosenblum, P. L. Choyke and H. Kobayashi, *Nat. Med.*, 2011, **17**, 1685–1691.
19 K. Stefflova, H. Li, J. Chen and G. Zheng, *Bioconjugate Chem.*, 2007, **18**, 379–388.
20 W. M. Sharman, J. E. van Lier and C. M. Allen, *Adv. Drug Delivery Rev.*, 2004, **56**, 53–76.
21 W. Li, S. Tan, Y. Xing, Q. Liu, S. Li, Q. Chen, M. Yu, F. Wang and Z. Hong, *Mol. Pharm.*, 2018, **15**, 1505–1514.
22 R. Mahato, W. Tai and K. Cheng, *Adv. Drug Delivery Rev.*, 2011, **63**, 659–670.
23 B. G. Muller, H. Leuenberger and T. Kissel, *Pharm. Res.*, 1996, **13**, 32–37.
24 C. Weber, J. Kreuter and K. Langer, *Int. J. Pharm.*, 2000, **196**, 197–200.
25 M. Wacker, K. Chen, A. Preuss, K. Possemeyer, B. Roeder and K. Langer, *Int. J. Pharm.*, 2010, **393**, 253–262.
26 M. T. Larsen, M. Kuhlmann, M. L. Hvam and K. A. Howard, *Mol. Cell. Ther.*, 2016, **4**, 3.
27 C. Yu, E. Xiao, P. Xu, J. Lin, L. Hu, J. Zhang, S. Dai, Z. Ding, Y. Xiao and Z. Chen, *RSC Adv.*, 2021, **11**, 7226–7230.
28 X. Li, Y. H. Jeon, N. Kwon, J. G. Park, T. Guo, H. R. Kim, J. D. Huang, D. S. Lee and J. Yoon, *Biomaterials*, 2021, **266**, 120430.
29 H. Liu, L. L. Lv, H. Wen, D. M. Zhao, J. Wu, M. R. Ke, B. Y. Zheng, J. Li, X. Li and J. D. Huang, *ACS Appl. Mater. Interfaces*, 2022, **14**, 28581–28590.
30 K. Ding, L. Wang, J. Zhu, D. He, Y. Huang, W. Zhang, Z. Wang, A. Qin, J. Hou and B. Z. Tang, *ACS Nano*, 2022, **16**, 7535–7546.
31 S. M. Usama and K. Burgess, *Acc. Chem. Res.*, 2021, **54**, 2121–2131.
32 S. M. Usama, C. M. Lin and K. Burgess, *Bioconjugate Chem.*, 2018, **29**, 3886–3895.
33 A. O. Elzoghby, M. M. Elgohary and N. M. Kamel, *Adv. Protein Chem. Struct. Biol.*, 2015, **98**, 169–221.
34 J. Vaz, D. Ansari, A. Sasor and R. Andersson, *Pancreas*, 2015, **44**, 1024–1035.
35 Z. Sheng, D. Hu, M. Zheng, P. Zhao, H. Liu, D. Gao, P. Gong, G. Gao, P. Zhang, Y. Ma and L. Cai, *ACS Nano*, 2014, **8**, 12310–12322.
36 U. Prabhakar, H. Maeda, R. K. Jain, E. M. Sevick-Muraca, W. Zamboni, O. C. Farokhzad, S. T. Barry, A. Gabizon, P. Grodzinski and D. C. Blakey, *Cancer Res.*, 2013, **73**, 2412–2417.
37 Y. Matsumura and H. Maeda, *Cancer Res.*, 1986, **46**, 6387–6392.
38 I. Yoon, J. Z. Li and Y. K. Shim, *Clin. Endosc.*, 2013, **46**, 7–23.
39 H. L. Wang and T. W. Lai, *Sci. Rep.*, 2014, **4**, 6588.
40 P. W. Hamer, J. M. McGeachie, M. J. Davies and M. D. Grounds, *J. Anat.*, 2002, **200**, 69–79.